

Universal path decomposition of multilayer transfer and scattering matrices

Joaquin Garcia-Suarez¹

¹*Institute of Civil Engineering, École Polytechnique Fédérale de Lausanne (EPFL),
CH-1015 Lausanne, Switzerland*

Abstract

We report a universal identity: any entry of a one-dimensional transfer or scattering matrix comprising N layers equals a coherent sum of 2^{N-1} directed paths representing wave patterns with pre-defined amplitude and phase evolutions. Treating those paths as analytic building blocks, we derive closed-form results for arbitrary stratified media — optical, acoustic, elastic, or electronic — without resorting to matrix products or recursion. The combinatorial construction of paths turns layered system design into rule-based path engineering, illustrated with a design example that offers a reinterpretation of the quarter-wavelength principle. We also quantify the computational speed-up of the path method over classical transfer-matrix chaining and showcase two more cross-disciplinary applications (site-response seismology and quantum superlattices). This paradigm replaces numerical sweeps that employ the transfer matrix method with physically-transparent path-construction rules, its applicability spans across physical disciplines and scales: from nanometer optical coatings to kilometer-scale seismic strata.

Introduction

Understanding wave propagation in layered systems is essential for design and optimization in a wide range of subjects, such as phononic [1] and photonic

¹Corresponding author: joaquin.garciasuarez@epfl.ch

crystals [2], elastodynamics [3], acoustic metamaterials [4], and quantum superlattices [5]. These systems often rely on engineered interference, bandgap formation, or resonance phenomena that emerge from the interaction of superimposing waves. Accurately predicting how linear waves reflect, transmit, or localize within such architectures is essential for tailoring their functional properties. This capability underpins a wide range of applications, including sound insulation [6, 7], inverting the path of seismic waves from the mantle to the ground surface [8, 9] and design of earthquake barriers [10], laser control [11], analog computers [12], and devices that tune electronic and heat transport [13, 14]. Performing the necessary calculations, especially in complex or highly heterogeneous systems, relies on the transfer matrix approach [15, 16, 17, 18, 19, 20, 21], which is both mathematically and physically sound, and robust and efficient from the computational implementation standpoint.

Both “transfer” matrices (also termed “propagators”) and “scattering” matrices are used to analyze wave propagation in stratified media. The difference between the two is that transfer matrices relate wave amplitudes across sections of the medium (making them ideal for modeling periodic structures and computing dispersion relations), while scattering matrices relate incoming to outgoing waves in a stack (thus providing direct access to reflection and transmission coefficients across the stack). Transfer matrices are widely used across a number of branches of computational physics for forward modeling and band structure analysis, whereas scattering matrices are employed in inverse problems. The entries in the transfer matrix can also be interpreted as a general form of the impulse response (Green’s function) for the propagation of linear waves in 1D layered media [9].

A closed-form expression for the transfer (scattering) matrix of an arbitrary number of layers has remained elusive [22, 23, 24], forcing designers to rely primarily on numerical parametric analyses to evaluate the relative significance of various parameters. In this contribution, we define a “path” as an ordered sequence of reflection and transmission events experienced by a steady-state harmonic disturbance within a heterogeneous medium composed of homogeneous layers separated by sharp interfaces; we show that any field within the composite

medium can be expressed as a finite superposition of these paths. Starting with the familiar 2×2 one-layer transfer matrix, we interpret its entries as impulse response in a 1D homogeneous medium; then, with the two-layer stack, we show that the cumulative transfer matrix equals the coherent sum of the two admissible paths, thereby exposing a direct link between algebraic results and wave amplitudes in the system. Generalizing this construction, we show that an N -layer structure contains exactly 2^{N-1} such paths and that their superposition furnishes a closed-form expression for the transfer matrix entries; the scattering matrix follows immediately via a linear transformation. The next section illustrates the paradigm’s scope by (i) demonstrating a speed-up analysis that reaches two orders-of-magnitude gains, (ii) extending the quarter-wavelength principle and applying path-based rules to a three-layer Bragg mirror design, (iii) carrying out a faster seismic site-inversion example, and (iv) a quantum superlattice design. The following main result culminates previous work that managed to derive the “harmonic decomposition” for the transfer matrices used in phononics and geotechnical earthquake engineering through purely algebraic means [25, 26, 27] but lacked a physical rationale grounded in wave dynamics.

Results

Main result

Path-Sum Decomposition

Any entry of the transfer matrix \mathbf{T} or scattering matrix \mathbf{S} for a one-dimensional layered medium with N layers can be written as a sum over the 2^{N-1} steady-state interference wave patterns termed “paths”. For example, the upper-left entry of the scattering matrix takes the form:

$$S_{11} = \sum_{j=1}^{2^{N-1}} \mathcal{S}_j e^{-i\phi_j},$$

where \mathcal{S}_j and ϕ_j denote, respectively, the amplitude and phase shift accumulated along the j -th path and have a simple closed form (see below).

Implications of main result

This identity reveals that wave propagation in any stratified one-dimensional medium — whether electromagnetic, acoustic, elastic, or quantum — can be understood as a finite sum of contributions with a clear physical meaning: each term corresponds to a specific sequence of propagation plus transmission and reflection events across interfaces, whose amplitude and phase changes can be computed beforehand in closed-form. The closed-form path decomposition offers a physically transparent alternative to traditional matrix methods, eliminating the need for chain-multiplying matrices and enabling elementary, wave-based reasoning in place of abstract algebra. Rather than relying on numerical sweeps across the parameter space, this framework allows to analytically explore the behavior of arbitrary multilayer stacks by explicitly selecting or canceling families of paths. Crucially, the decomposition yields closed-form expressions valid for any sequence of layers and parameter combinations, allowing exact gradients to be computed analytically. This capability opens the door to gradient-based

optimization, in contrast to costly approaches such as memetic algorithms [28], genetic algorithms [29], or high-dimensional surrogate models like neural networks [30, 31].

Derivation of explicit expression of paths, plus phase and amplitude changes

Symbol	Meaning
N	Number of layers in the stack
l_i	Thickness of layer i
c_i	Wave speed in layer i
k_i	Wavenumber in layer i – see also Table 2
φ_j	Total phase accumulated along path j
t_i	Travel time across layer i , $t_i = l_i/c_i$
\mathbf{e}_j	Vector encoding direction (± 1) of wave in each layer along path j
Ψ	Vector of added phases (one entry per layer)
\mathbf{t}	Vector of travel times (one entry per layer)
\mathcal{A}_j	Coefficient of magnitude of the amplitude path j
\mathcal{A}'_j	Coefficient of magnitude of the gradient path j
\mathcal{S}_j	Symmetric part of scattering amplitude from path j
\mathcal{R}_j	Antisymmetric part of scattering amplitude from path j

Table 1. **List of symbols.** Notation used in the path decomposition of transfer and scattering matrices.

Table 1 presents the symbols used in the rest of the paper. To derive the main result from fundamental wave principles, we start with a physical interpretation of the “atomic” transfer matrices as representation of an impulse in a homogeneous layer. Consider a steady-state 1D scenario in frequency domain. An impulse at position $x = 0$ (i.e., 1 in frequency domain) is made up by two superimposing waves in a homogeneous layer, a left-propagating one (e^{-ikx}) and a right-propagating one (e^{ikx}):

$$\frac{1}{2}e^{ikx} + \frac{1}{2}e^{-ikx} = \cos(kx) , \quad (1)$$

where $i = \sqrt{-1}$ is the imaginary unit, k is the wavenumber of each harmonic and each exponential corresponds to a phase shift $\pm kx$, i.e., the wave oscillating and moving from $\pm x$ to 0. See Figure 1a and b for a visual depiction. We label this “superposition of symmetric phases” associated to the unitary amplitude “the path” of the impulse. For the homogeneous medium, the path can be thought as the phase and amplitude combinations in frequency domain that render a unitary amplitude wave. The gradients associated with the two new waves in Equation (1) therefore are

$$\frac{ik}{2}e^{ikx} - \frac{ik}{2}e^{-ikx} = -k \sin(kx) . \quad (2)$$

We now relate Equations (1) and (2) with the transfer matrix, \mathbf{T} , which connects the original impulse to the evolution along the path; symbolically: $[\text{amplitude, gradient}]_{x=x}^\top = \mathbf{T}(x, 0) [\text{amplitude, gradient}]_{x=0}^\top$. The terms “amplitude” and “gradient” generically denote pairs of wave variables that are continuous across interfaces; Table 2 lists representative examples across physical theories. Mirroring Equation (1), T_{11} gives us the new amplitudes associated to an impulse, while T_{21} is the gradient created by such an impulse, and it is reflected in Equation (2). The same reasoning tells that an impulse in the gradient means $\cos(kx) = T_{22}$, while the associated amplitude must be $\sin(kx)/k = T_{12}$ (since $dT_{12}/dx = T_{22}$). Thus we have derived the transfer matrix for one homogeneous layer:

$$\mathbf{T} = \begin{bmatrix} \cos(kx) & \frac{\sin(kx)}{k} \\ -k \sin(kx) & \cos(kx) \end{bmatrix} . \quad (3)$$

For two layers, \mathbf{T} must be able to represent the state at the edge of the second layer after propagation in the first layer plus interaction with the interface, plus propagation in the second one. To do so, we must track all possible ways in which the two waves in each layer (left-going and right-going) can interact with each other. The first layer is indexed with “1” and the second one with “2”. The resultant reflection/transmission at the interface of both amplitudes and gradients are proportional to the coefficients in Table 3. Each path originating

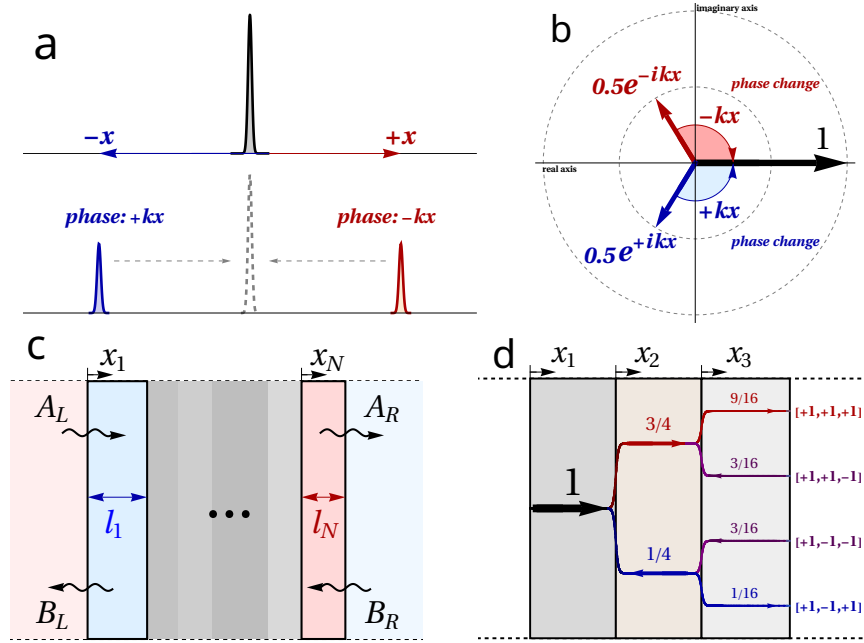


Figure 1. Conceptualize impulse amplitude as resultant of path. **a** An impulse in frequency domain can be regarded as two equal halves propagating in opposite directions superimposing at $x = 0$. **b** The path yields the zero phase unit from two halves corresponding to phase $\pm kx$. **c** Scheme of a stack within a layered medium in steady-state, each layer is spanned with $x_i \in [0, l_i]$, $i = 1, \dots, N$. The amplitude of the right-going and left-going at the left (right) edge are A_L and B_L (A_R and B_R), respectively. The fields in each layer that are represented in the transfer matrix always come from the superposition of one left-propagating contribution plus a right-propagating one. **d** Paths for an impulse across a three-layer laminate, assuming $k_1/k_2 = 1/2$ and also $k_2/k_3 = 1/2$: the initial amplitude is split in two pieces (number on top is their magnitude) in the second layer, each splitting in two in turn, thus giving rise to four potential paths. The paths are not rays, but resulting wave patters in frequency domain.

System	Amplitude	Gradient	Wavenumber
1D Shear Waves	tangential displacement	shear stress	$\frac{\omega}{\sqrt{G/\rho}}$
Acoustic Waves	longitudinal displacement	pressure	$\frac{\omega}{\sqrt{B/\rho}}$
Electromagnetic Waves	electric field	electric field gradient	$\omega\sqrt{\mu\epsilon}$
Electronics (Schrödinger Eq.)	wavefunction amplitude	wavefunction gradient	$\sqrt{\frac{2m(E - V)}{\hbar^2}}$

Table 2. **What does this work encompass?** Amplitude and gradient for relevant 1D wave systems. ω represents the frequency all the wave in all cases. G is the shear modulus of an elastic medium and B is the bulk modulus of an acoustic one. μ is the permeability and ϵ the permittivity of an electromagnetic medium. E is the total energy of a quantum wave-particle, m is its mass, \hbar is the reduced Planck constant and V is the potential well intensity. The explicit form of the transfer matrix can be found in the SI.

in 1 will accumulate phase proportional to the trip across 1, then it will interact (reflection and transmission) with the interface between 1 and 2; waves in 2 likewise have phase proportional to the trip across 2, the sign of the phase depending on if the the wave is going in the right direction or in the opposite one. Let l_1 be the width of layer 1 and l_2 the width of layer 2; if we continue to interpret paths in terms of phase and amplitude changes, as before, two natural candidates emerge by analogy.

- Path I: “composition of waves in 1 and 2 going in the same direction” (nicknamed “[+1, +1]”). The proportion of total amplitude is $1/T_{1 \rightarrow 2}$ (no direction change). The wave picks same-sign phase along, i.e., $\pm(k_1 l_1 + k_2 l_2)$.

Phenomenon	Coefficient	Expression	Alternative Form
Amplitude transmission	$T_{1 \rightarrow 2}$	$\frac{2k_2}{k_1 + k_2}$	$\frac{2}{1 + \frac{k_1}{k_2}}$
Amplitude reflection	$R_{1 \rightarrow 2}$	$\frac{k_2 - k_1}{k_1 + k_2}$	$\frac{T_{1 \rightarrow 2}}{2} \left(1 - \frac{k_1}{k_2}\right)$
Gradient transmission	$T'_{1 \rightarrow 2}$	$\frac{k_1}{k_2} T_{1 \rightarrow 2}$	$\frac{2}{1 + \frac{k_2}{k_1}}$
Gradient reflection	$R'_{1 \rightarrow 2}$	$-R_{1 \rightarrow 2}$	$\frac{T'_{1 \rightarrow 2}}{2} \left(1 - \frac{k_2}{k_1}\right)$

Table 3. **Transmission and reflection coefficients.** For an interface between layers with wavenumbers k_1 and k_2 , for both amplitude and gradient continuity. Notice that reversing the order of the layers in $T_{1 \rightarrow 2}$ and $R_{1 \rightarrow 2}$ yields $T'_{1 \rightarrow 2}$ and $R'_{1 \rightarrow 2}$. To recover the standard Fresnel coefficients for rays, note that impedance is inversely proportional to the wavenumber.

Similarly to Equation (1), this would correspond to

$$\frac{1}{T_{1 \rightarrow 2}} \left(\frac{1}{2} e^{i(k_1 l_1 + k_2 l_2)} + \frac{1}{2} e^{-i(k_1 l_1 + k_2 l_2)} \right) = \frac{1}{T_{1 \rightarrow 2}} \cos(k_1 l_1 + k_2 l_2) . \quad (4)$$

- Path II: “composition of waves in opposite directions” (“ $[+1, -1]$ ”). The proportion of total amplitude is $R_{1 \rightarrow 2}/T_{1 \rightarrow 2}$ (one change of direction). Phase change $\pm(k_1 l_1 - k_2 l_2)$.

$$\frac{R_{1 \rightarrow 2}}{T_{1 \rightarrow 2}} \left(\frac{1}{2} e^{i(k_1 l_1 - k_2 l_2)} + \frac{1}{2} e^{-i(k_1 l_1 - k_2 l_2)} \right) = \frac{R_{1 \rightarrow 2}}{T_{1 \rightarrow 2}} \cos(k_1 l_1 - k_2 l_2) . \quad (5)$$

Thus the amplitude response in the second layer to an amplitude impulse at the first layer of the medium, T_{11} , is the sum of the two possible paths, (4) plus (5). For T_{22} we can use similar arguments (gradient response at the end of the second layer to a gradient impulse at the initial edge of the stack), but with the proper transmission/reflection coefficients, $T'_{1 \rightarrow 2}$ and $R'_{1 \rightarrow 2}$, recall Table 3. Analogously to Eq. (2), the term T_{21} must capture the gradient associated with T_{11} in the second layer. This corresponds to a phase shift of $-\pi/2$ and an amplitude scaling proportional to the wavenumber in the final layer. Similarly, T_{12} must represent the amplitude in the second layer resulting from a gradient impulse—equivalently,

a phase shift of $+\pi/2$ and an amplitude scaling proportional to the inverse of the final-layer wavenumber. In summary, the transfer matrix for two layers is

$$\mathbf{T} = \begin{bmatrix} \frac{1}{\bar{\tau}_{1 \rightarrow 2}} \cos(k_1 l_1 + k_2 l_2) & \frac{1}{k_2 \bar{\tau}'_{1 \rightarrow 2}} \sin(k_1 l_1 + k_2 l_2) \\ \frac{R_{1 \rightarrow 2}}{\bar{\tau}_{1 \rightarrow 2}} \cos(k_1 l_1 - k_2 l_2) & -\frac{R'_{1 \rightarrow 2}}{k_2 \bar{\tau}'_{1 \rightarrow 2}} \sin(k_1 l_1 - k_2 l_2) \\ \hline -k_2 \frac{1}{\bar{\tau}_{1 \rightarrow 2}} \sin(k_1 l_1 + k_2 l_2) & \frac{1}{\bar{\tau}'_{1 \rightarrow 2}} \cos(k_1 l_1 + k_2 l_2) \\ +k_2 \frac{R_{1 \rightarrow 2}}{\bar{\tau}_{1 \rightarrow 2}} \sin(k_1 l_1 - k_2 l_2) & +\frac{R'_{1 \rightarrow 2}}{\bar{\tau}'_{1 \rightarrow 2}} \cos(k_1 l_1 - k_2 l_2) \end{bmatrix}, \quad (6)$$

built directly from elementary operations. Expanding the sum in the cosines and substituting the coefficients in terms of the wavenumbers, we reach the form in which it is usually found in the literature (see, for instance, Refs. [32, 33, 21]) or if we had performed the matrix multiplication directly:

$$\begin{aligned} \mathbf{T} &= \begin{bmatrix} \cos(k_2 l_2) & \frac{\sin(k_2 l_2)}{k_2} \\ -k_2 \sin(k_2 l_2) & \cos(k_2 l_2) \end{bmatrix} \begin{bmatrix} \cos(k_1 l_1) & \frac{\sin(k_1 l_1)}{k_1} \\ -k_1 \sin(k_1 l_1) & \cos(k_1 l_1) \end{bmatrix} \\ &= \begin{bmatrix} \cos(k_2 l_2) \cos(k_1 l_1) & \cos(k_2 l_2) \frac{\sin(k_1 l_1)}{k_1} \\ -\frac{k_1}{k_2} \sin(k_2 l_2) \sin(k_1 l_1) & +\frac{\sin(k_2 l_2)}{k_2} \cos(k_1 l_1) \end{bmatrix} \\ &\quad \hline \begin{bmatrix} -k_2 \sin(k_2 l_2) \cos(k_1 l_1) & -\frac{k_2}{k_1} \sin(k_2 l_2) \sin(k_1 l_1) \\ -\cos(k_2 l_2) k_1 \sin(k_1 l_1) & +\cos(k_2 l_2) \cos(k_1 l_1) \end{bmatrix}. \end{aligned} \quad (7)$$

The equivalence between Equations (6) and (7) has always been there, yet veiled behind complicated-looking expressions whose physical meaning was not obvious.

The last step is just an inductive generalization. Each extra layer adds two new waves (left-going and right-going) to combine with, which doubles the number of possible paths, therefore for N layers and $N - 1$ interfaces the number of paths to account for is 2^{N-1} . See Figure 1d. The general transfer matrix can thus be written as a sum over all paths

$$\mathbf{T} = \sum_{j=1}^{2^{N-1}} \begin{bmatrix} \mathcal{A}_j \cos(\varphi_j) & \frac{e_{jN}}{k_N} \mathcal{A}'_j \sin(\varphi_j) \\ -e_{jN} k_N \mathcal{A}_j \sin(\varphi_j) & \mathcal{A}'_j \cos(\varphi_j) \end{bmatrix}, \quad (8)$$

where, following the previous two-layer example, the j -th path is identified with a vector \mathbf{e}_j containing one entry per layer (± 1) and which can be seen as the j -th

row of a matrix \mathbf{e} , whose entries are e_{ji} where $j = 1, \dots, 2^{N-1}$ and $i = 1, \dots, N$. The entry is $+1$ if the interaction is with the right-going wave in the layer, -1 if with the left-going one; since each sine or cosine contains also the exponential with all signs flipped, we can fix $e_{j1} = +1$ without loss of generality. Hence, the total phase change along the j -th path, φ_j , can be expressed as

$$\varphi_j = \mathbf{e}_j^\top \Psi = \sum_{i=1}^N e_{ji} k_i l_i, \quad (9)$$

where $\Psi = [k_1 l_1, \dots, k_N l_N]^\top$ is the vector of positive phase changes across each layer. The total magnitude change along the j -th path for amplitudes, \mathcal{A}_j , and gradients, \mathcal{A}'_j , are

$$\begin{aligned} \mathcal{A}_j &= \prod_{i=2}^N \frac{1}{T_{i-1 \rightarrow i}} \left(\frac{1 + R_{i-1 \rightarrow i}}{2} + e_{ji-1} e_{ji} \frac{1 - R_{i-1 \rightarrow i}}{2} \right) \\ &= \prod_{i=2}^N \frac{1}{2} \left(1 + e_{ji-1} e_{ji} \frac{k_{i-1}}{k_i} \right), \end{aligned} \quad (10a)$$

and

$$\begin{aligned} \mathcal{A}'_j &= \prod_{i=2}^N \frac{1}{T'_{i-1 \rightarrow i}} \left(\frac{1 + R'_{i-1 \rightarrow i}}{2} + e_{ji-1} e_{ji} \frac{1 - R'_{i-1 \rightarrow i}}{2} \right) \\ &= \prod_{i=2}^N \frac{1}{2} \left(1 + e_{ji-1} e_{ji} \frac{k_i}{k_{i-1}} \right), \end{aligned} \quad (10b)$$

which also depends on \mathbf{e}_j : namely, when two consecutive signs match, the wave continues in the same direction — i.e., a transmission event; when the signs differ, the wave changes direction, signaling a reflection. Because the coefficients \mathcal{A}_j would equal \mathcal{A}'_j under layer-order reversal, the entry T_{22} can be interpreted as T_{11} evaluated with the stack traversed in the opposite direction. Consequently, the trace $T_{11} + T_{22}$ represents the superposition of all amplitude paths, accounting for propagation through the stack in both directions simultaneously. Note also that $\sum_j \mathcal{A}_j = \sum_j \mathcal{A}'_j = 1$, i.e., the amplitudes must sum up to one, as the paths represent all the possible ways an impulse can be broken up. A purely algebraic proof of this result (without physical reasoning) inspired by Ref.[27] is also included in the SM.

Having the transfer matrix, one can compute the N -layer scattering matrix, \mathbf{S} , which represents the stack whose inputs are A_L coming from the left in the first layer at $x_1 = 0$ and B_R coming from the right into the last layer at $x_N = 0$, Figure 1c. \mathbf{S} can be written in terms of the N -layer transfer matrix [19] using a linear transformation, so, since all its entries can be written in terms of those of \mathbf{T} , \mathbf{S} also admits a path decomposition:

$$\mathbf{S} = \sum_{j=1}^{2^N-1} \left(\mathcal{S}_j \begin{bmatrix} e^{-i\epsilon_{jN}\varphi_j} & 0 \\ 0 & e^{i\epsilon_{jN}\varphi_j} \end{bmatrix} + \mathcal{R}_j \begin{bmatrix} 0 & e^{-i\epsilon_{jN}\varphi_j} \\ e^{i\epsilon_{jN}\varphi_j} & 0 \end{bmatrix} \right), \quad (11)$$

where the amplitudes \mathcal{S}_j and \mathcal{R}_j depend on the impedance of the interfaces and the wavenumber ratio between the first and the last layer:

$$\mathcal{S}_j = \frac{1}{2} \left(\mathcal{A}_j + \frac{k_1}{k_N} \mathcal{A}'_j \right), \quad \mathcal{R}_j = \frac{1}{2} \left(\mathcal{A}_j - \frac{k_1}{k_N} \mathcal{A}'_j \right). \quad (12)$$

The coefficients of the scattering matrix in turn define the transmitted and reflected amplitudes for classical waves [8, 34], or the probability of reflection or transmission of quantum particles at energy barriers [35].

Application example: design rules for Bragg mirrors

The path decomposition can help to reinterpret classic results in wave propagation. As an illustrative example from electromagnetism, consider the well-known quarter-wavelength ($\lambda/4$) rule in optics. This principle is commonly used in the design of dielectric mirrors [36] and states that, at a given design frequency, ω_{design} , each material layer should be made a quarter of the local wavelength in thickness, i.e., $l_i = \lambda_i/4 = \pi/2k_i$ for $i = 1, \dots, N$, where λ_i and k_i are the wavelength and wavenumber in the i -th material, respectively. This choice simplifies the design process: at ω_{design} , each layer introduces a phase shift of exactly $\pm\pi/2$. As a result, the layers act as modular building blocks — each contributing the same phase — thereby simplifying their combination to achieve desired optical properties through constructive or destructive interference. The claim we make here is that the $\lambda/4$ rule applied to the design of a two-layer dielectric mirror is equivalent maximizing the amplitude of the two paths for the design frequency.

The goal is to design a dielectric mirror with a stop-band at a given design frequency, $\omega_{\text{design}} = 500 \text{ THz}$ (wavelength 600 nm). Let us review first some necessary concepts. Given the wave speed of the j -th layer, c_j , the oscillation frequency $\omega = k_j c_j = k_j c_0 / n_j$ (c_0 being the light speed in vacuum and n_j the refractive index in the medium), which can be seen as a constant across layers independent from material properties. The phase associated to the i -th path, Equation (9), can hence be expressed in terms of the travel time in each layer as

$$\varphi_i = \omega \tau_i, \quad \text{where } \tau_i = \mathbf{e}_j^\top \mathbf{t}, \quad \text{and } \mathbf{t} = [l_1/c_1, \dots, l_N/c_N]^\top. \quad (13)$$

Notice that φ_j is either 0 or π (modulo 2π) at ω_{design} , for any even N . Using Equations (4) and (5),

$$\text{Path I : } \frac{1}{T_{1 \rightarrow 2}} \cos(\omega_{\text{design}}(t_1 + t_2)) = \frac{1}{T_{1 \rightarrow 2}} \cos(\pi) = -\frac{1}{T_{1 \rightarrow 2}} = -\frac{1}{2} \left(1 + \frac{n_2}{n_1}\right), \quad (14a)$$

$$\text{Path II : } \frac{R_{1 \rightarrow 2}}{T_{1 \rightarrow 2}} \cos(\omega_{\text{design}}(t_1 - t_2)) = \frac{R_{1 \rightarrow 2}}{T_{1 \rightarrow 2}} \cos(0) = +\frac{R_{1 \rightarrow 2}}{T_{1 \rightarrow 2}} = \frac{1}{2} \left(1 - \frac{n_2}{n_1}\right), \quad (14b)$$

i.e., the amplitude of I at the end of the second layer is as negative as it can be while the amplitude of II is maximum too but its sign will depend on the relation between n_2 and n_1 (actually, the value is the same for any frequency, not only the ω_{design}). The result of the path superposition at the design frequency only depends on the ratio of the indexes; take (as it is customary) $n_2/n_1 \gg 1$, then the amplitude of the second one is also negative, so the amplitude contribution of each cell has equal sign and the sum of the two renders $T_{11}(\omega_{\text{design}}) \approx -n_2/n_1$. The dispersion relation is controlled by the trace of the transfer matrix [32, 34, 37] (see also Methods below), i.e., only frequencies that yield a value of the trace smaller than 2 can propagate in the stratified medium. To compute the trace of \mathbf{T} , T_{22} is also required; owing to the symmetries in Table 3 we know right away that $T_{22}(\omega_{\text{design}}) = -n_1/n_2 \ll 1$; thus, the trace can be approximated simply by $-n_2/n_1$. The skin depth [38] is thus $L_p = (l_1 + l_2) / \ln(n_2/n_1)$, a result reached solely using paths. Figure 2 presents the results for a two-layer dielectric

mirror that targets the wavelength 600nm (500THz), including verification using the transfer matrix method. By decomposing each path in amplitude, Equation (10b), and period, Equation (13), and combining these into a single concept, we can define the “spectrum of the dispersion relation” (Figure 2b) symbolically $\{\tau_j, \mathcal{A}_j\}_{j=1}^{2^N-1}$.

The path decomposition allows us to go beyond the $\lambda/4$ rule and explore alternative design guidelines for dielectric mirrors that minimize penetration length by maximizing the trace of the transfer matrix at the design frequency. For instance:

1. Choose the refraction indexes to maximize the magnitude of a subset of paths for a given design frequency.
2. Choose the layer widths to ensure that those paths add up constructively to maximize the trace at the design frequency while the others remain negligible.

We apply these rules to the inverse design of a three-layer unit cell at 600nm - 500THz - again. In this case there are four paths to define, see Figure 1d. Pick the phases so that (just like in the two-layer case) the last path provides constant amplitude: $\omega t_1 = \omega t_2 + \omega t_3$ ($\varphi_1 = 2\omega t_1$, $\varphi_4 = 0$) and for simplicity also $\omega t_2 = \omega t_3 = \omega t_1/2$ ($\varphi_2 = \omega t_1$, $\varphi_3 = \omega t_1$), thus:

$$\text{I : } \frac{1}{T_{1 \rightarrow 2}} \frac{1}{T_{2 \rightarrow 3}} \cos(2\omega t_1) = \frac{1}{4} \left(1 + \frac{n_2}{n_1} \right) \left(1 + \frac{n_3}{n_2} \right) \cos(2\omega t_1), \quad (15a)$$

$$\text{II : } \frac{1}{T_{1 \rightarrow 2}} \frac{R_{3 \rightarrow 3}}{T_{2 \rightarrow 3}} \cos(\omega t_1) = \frac{1}{4} \left(1 + \frac{n_2}{n_1} \right) \left(1 - \frac{n_3}{n_2} \right) \cos(\omega t_1), \quad (15b)$$

$$\text{III : } \frac{R_{1 \rightarrow 2}}{T_{1 \rightarrow 2}} \frac{R_{2 \rightarrow 3}}{T_{2 \rightarrow 3}} \cos(\omega t_1) = \frac{1}{4} \left(1 - \frac{n_2}{n_1} \right) \left(1 - \frac{n_3}{n_2} \right) \cos(\omega t_1), \quad (15c)$$

$$\text{IV : } \frac{R_{1 \rightarrow 2}}{T_{1 \rightarrow 2}} \frac{1}{T_{2 \rightarrow 3}} \cos(0) = \frac{1}{4} \left(1 - \frac{n_2}{n_1} \right) \left(1 + \frac{n_3}{n_2} \right). \quad (15d)$$

Assume $n_2/n_1 > 1$ and $n_3/n_2 < 1$ (low-high-low refraction index sequence), thus the amplitude of IV is guaranteed to be negative. Next, pick l_1 so that at the design frequency $\cos(2\omega t_1) = -1 \rightarrow 2\omega t_1 = 2k_1 l_1 = 4\pi l_1/\lambda_1 = \pi \rightarrow l_1 = \lambda_1/4$ (which guarantees that the first path at the design frequency attains the most negative amplitude possible), while it follows that $l_2 = \lambda_2/8$ and $l_3 = \lambda_3/8$ as

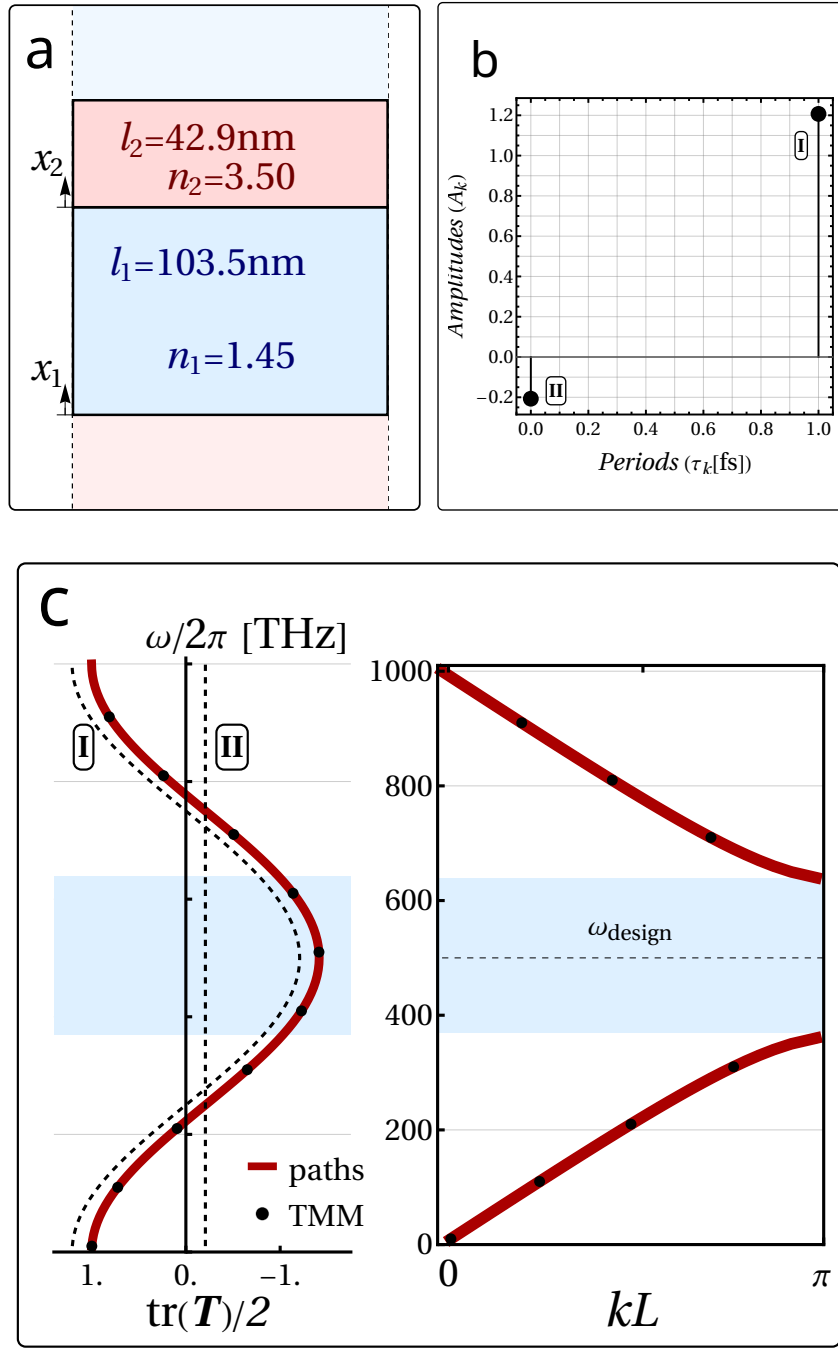


Figure 2. **Spectrum of the dispersion relation of a dielectric mirror.** **a** Scheme of the unit cell. **b** Spectrum of the half-trace function, which in turn is equivalent to the dispersion relation, with each path contribution labeled (I and II). **c** Plot of the half-trace function and the dispersion relation as a function of frequency ω , the two labeled dashed lines represent the two paths in the spectrum (as functions of ω) whose superposition renders the half-trace function. Shaded regions correspond to $|\text{tr}(\mathbf{T}(\omega))/2| > 1$, i.e., stop-bands. “TMM” represents numerical results from the transfer matrix method.

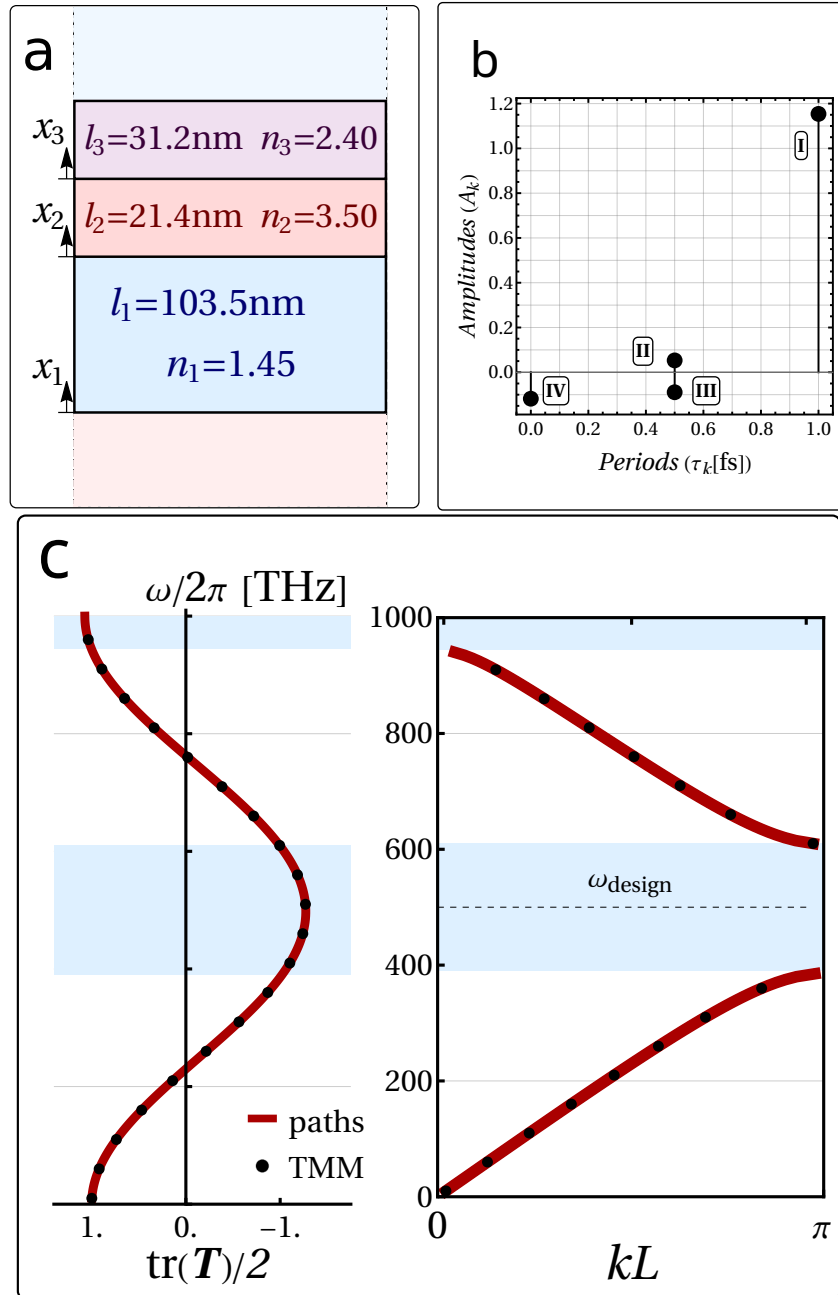


Figure 3. **Dielectric mirror with three subcomponents.** **a** Scheme of the unit cell. **b** Spectrum of the half-trace function, with each path contribution labeled (I, II, III and IV). **c** Plot of the half-trace function and the dispersion relation as a function of frequency ω , shaded regions correspond to stop-bands. “TMM” represents numerical results from the transfer matrix method.

well (which guarantees that the amplitude of the two intermediate paths at the design frequency is zero). Therefore, in this example with odd number of layers, the width is $\lambda/4$ in the first layer and $\lambda/8$ in the second and third. The design and results are included in Figure 3. This exercise highlights physical insights obtained from leaning into a path-based understanding, but the method offers also numerical advantages.

Numerical performance benchmarking

The path decomposition not only brings new physical insights but also provides an alternative for transfer matrix method (TMM). The relative independence of each path makes their evaluation suitable for vectorization, as opposed to TMM which is inherently sequential. Figure 4 displays the numerical comparison in terms of runtime (for details on the hardware used, see Methods), the test consisted in evaluating T_{11} for a list of 9950 input values (wavenumbers) using both methods and recording the time that each took to complete the task as a function of the number of layers, N .

The TMM is a sequential method; the path decomposition, by contrast, enables not only vectorization but also explicit control over computational effort through the choice of the number of paths that are evaluated. The parameter of choice to truncate the series is not the amplitude magnitude (it would require computing all the paths and then identifying those) but the number of reflections in each path, M , which is but the number of sign changes in the corresponding path-defining vector \mathbf{e}_j . Due to the combinatorial structure of the system, the paths can be computed sequentially from $M = 0$ ($\mathbf{e}_j = [+1, \dots, +1]$) to the maximum M chosen by the user.

From Figure 4a, we acknowledge that TMM scales linearly with N , while the full path enumeration becomes impractical for $N \approx 15$ since the number of operations necessary increases exponentially. Luckily, Figure 4b, the truncated decompositions with small M remain efficient, even for large N , as the the number of operations to evaluate the truncated paths scales polynomially with N (see also Methods for the operation-count estimation). The trade-off is that

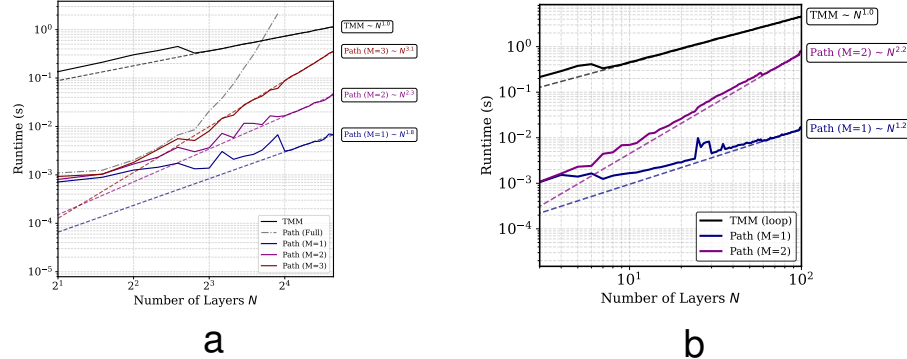


Figure 4. (a) Raw runtimes for different methods as a function of number of layers (small number of layers). (b) Same data with trend line overlays showing asymptotic scaling (up to 100 layers).

one loses some precision due to truncation errors, this is shown by the following application example. As take-away:

- The full path-decomposition can easily be at least $10\times$ faster for small number of layers ($N \leq 8$).
- The truncated path-decomposition can be competitive for large number of layers (dozens) if picking $M \ll N$ is allowed by the problem.
- In best case scenarios, the path-based vectorized approach can deliver speedups over TMM in the order of $100\times$.

Application example: soil site inversion

The Kik-Net station **fksh14** [39] is modelled with four soil layers over half-space, see Figure 5a. The transfer function relating the amplitude of bedrock motion to the amplitude at ground level is equal to the inverse of $T_{11}(\omega)$ [26]. Figure 5b compares transfer functions obtained with path truncation ($M = 0\text{--}3$) against the reference TMM result; the curve for $M = 1$ (4 of 8 paths) is already close enough to the data so that resonance frequencies could be estimated.

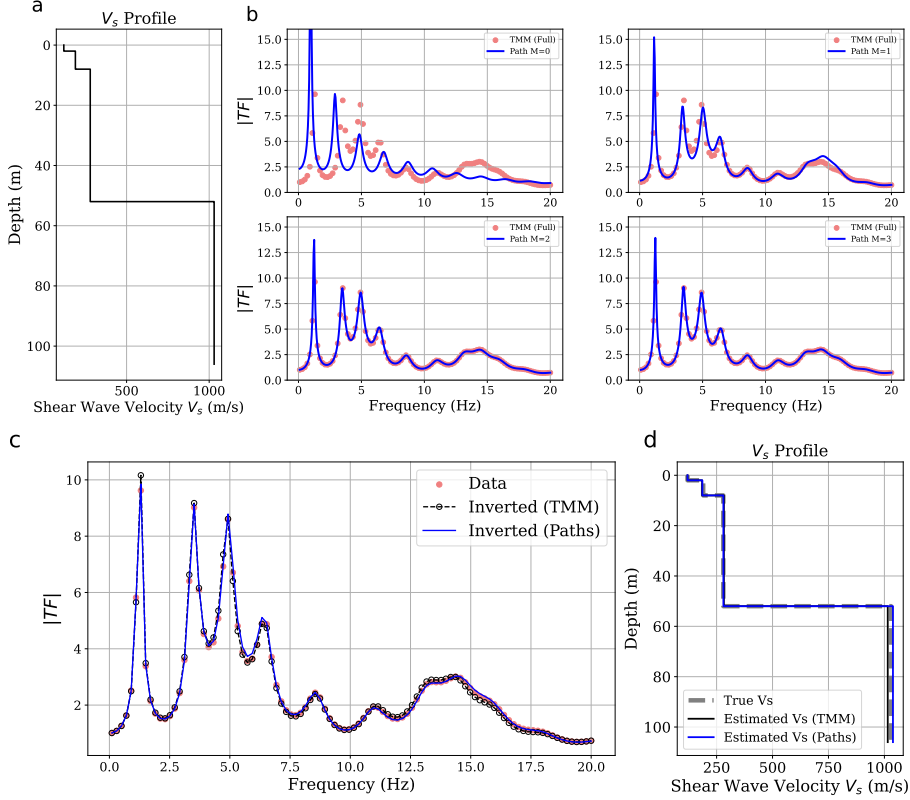


Figure 5. Using transfer function to asses applications of path decomposition in seismology. **a** Soil site shear wave velocity profile corresponding to Kik-Net station fksh14. **b** Convergence of transfer functions using path-truncation to results from TMM: $M = 0$ (1 out of 8 paths), $M = 1$ (4 out of 8 paths), $M = 2$ (7 out of 8 paths), $M = 3$ (8 out of 8 paths). **c** Amplitude-frequency data and reconstructed transfer function using global inversion techniques (forward simulations run either with TMM or full path decomposition). The procedure using TMM takes ≈ 5.3 seconds, versus 0.06 seconds using the vectorized path evaluation (91 \times speedup). **c** **d** Inverted soil profiles versus true profile.

Using the same global optimizer, we fit the measured amplitude spectrum with two forward solvers: TMM and the full path sum. Both return nearly identical transfer functions (Figure 5c) and velocity profiles (Figure 5d), but the path solver completes in 0.06 s versus 5.3 s for TMM (400 frequencies, 500 iterations), a 91 \times speed-up consequence of the performance gains discussed in the prior sections. This showcases how evaluation of paths can replace TMM to

speed traditional methods up, in the next section we will see how the analytical path decomposition allows to tackle an optimization problem in layered media using (numerical) gradients, i.e., local search methods.

Application example: gradient-based optimization of quantum superlattice

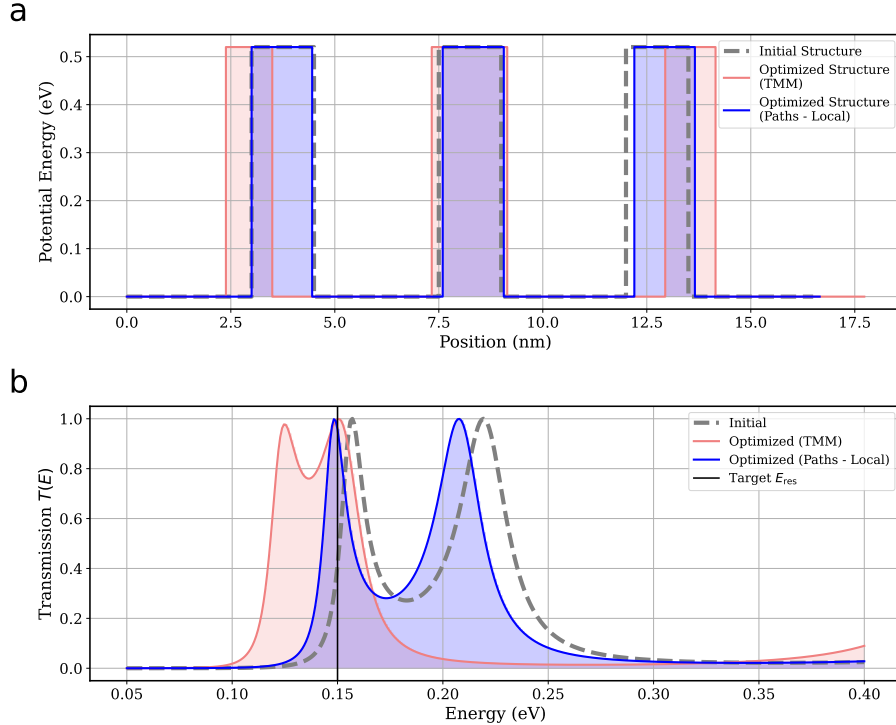


Figure 6. **Gradient-based optimization of quantum well-barrier lattice.** **a** Initial (regular) distribution of potential wells and barriers, as well as optimized ones to match 95% transmission at the 0.15 eV (optimization with TMM uses global search method, while optimization with paths uses local gradient-based search). **b** Transmission spectrum: initial and optimized ones.

The path formulation is not only faster than TMM; its closed form also provides gradients of the variable of interest directly, which makes local optimization feasible. We apply this to a seven-layer GaAs/AlAs superlattice whose initial well/barrier thicknesses are 3.0 nm and 1.5 nm. The task is to reach 95 % transmission at 0.15 eV.

Using TMM we rely on a global differential-evolution search. With the path sum, we can (for the first time) compute finite-difference gradients of the relevant magnitude and run a BFGS update.

Discussion

The path decomposition emerged as an unexpected result during the investigation of a general structure for the transfer matrix [25]. This development originated from a series of mathematical manipulations carried out without an initial focus on the physical interpretation of the intermediate expressions; serendipitously, the mathematical outcome provided a solid foundation that has allowed the path-sum physical interpretation to be reconstructed retrospectively with confidence on its ultimate validity. This physical interpretation has taken a number of iterations to mature. Initially, we attempted to interpret the result in terms of rays; however, this notion was ultimately dismissed due to the derivation being carried out in the frequency domain. Instead, the current picture regards the paths as steady-state, stationary-phase wave patterns that serve as a basis for representing any possible field within a N -layer composite medium. Our main result parallels other sum-over-histories pictures [40], yet in stratified 1D media the “histories” would be ray loops that collapse to a finite set of paths whose amplitudes can be added exactly, yielding the closed-form expressions presented earlier.

From a computational standpoint, the contrast between methods is striking: the classical transfer-matrix chain scales linearly with the number of layers $\sim N$, whereas the full path-sum grows exponentially $\sim 2^N$ and quickly becomes intractable. Truncating the path catalogue to at most M internal reflections reforms this exponential wall into a controllable polynomial cost $\sim N \times P_M(N)$ – where $P_M(N) = \sum_{r=0}^M \binom{N-1}{r}$ – allowing practitioners to trade accuracy for speed in a transparent way. Because every term in the truncated series is analytic in the layer parameters, the framework also lends itself to differentiation, opening the door to powerful gradient-based design loops (demonstrated in the quantum

superlattice optimization).

Future work should aim to extend the path-sum decomposition to account for oblique incidence and material dissipation, broadening its applicability. Beyond forward modeling, the decomposition also presents an alternative framework for inverse design. By expressing the response as a sum over physically interpretable paths, it becomes possible to engineer spectral features analytically — selecting and shaping dominant contributions rather than relying on numerical parameter sweeps. The formulation also facilitates detailed parameter sensitivity analysis, making it possible to compute exact gradients of any transfer matrix entry with respect to layer thicknesses, material parameters, or even the number of layers (through finite differences). The optical examples presented here offer only a first glimpse of the broader potential of this approach. The potential concern as to exploding complexity — since the number of paths increases exponentially with the number of layers — is mitigated as it is apparent that only a small portion of paths will control the overall response, e.g., in Figures 2 and 3, see how the most relevant paths (those that feature largest amplitudes) are easily distinguished from the rest.

The relevance of this contribution is further underscored by very recent efforts in the phononics community [1] which highlight the need for physically transparent, generalizable approaches to wave control and dynamic homogenization. Our path-decomposition framework offers such a foundation in one dimension, enabling a fully analytic treatment of multilayer scattering and its direct integration into design workflows. Beyond this, the analytic perspective provides a natural lens through which to chart and potentially optimize the boundaries of this design space, prompting questions such as: with N layers in a unit cell, what is the shortest achievable penetration depth? How wide can a stop-band be made, and how low can its opening frequency drop? How densely can stop-bands be packed across a given spectral range, and what trade-offs arise between bandwidth, number of gaps, and unit-cell complexity? The path decomposition offers a toolkit for exploring such questions.

Methods

General matrix expressions

Starting from the PDE that governs wave propagation, through either Fourier transform or a plane-wave expansion and dividing the problem in frequency domain into “amplitude” and “gradient”, one reaches a linear first-order vector ODE (see SM for details). Let f be the amplitude of the field of interest and f' its gradient, gather them in a vector $[f(x, k), f'(x, k)]^\top$. The solution for a perturbation propagating across a homogeneous medium along the x -direction is governed by the map [19, 20, 41]

$$\begin{bmatrix} f \\ f' \end{bmatrix}_{x=x_{i+1}} = \mathbf{T}(x_{i+1}, x_i) \begin{bmatrix} f \\ f' \end{bmatrix}_{x=x_i} = \begin{bmatrix} \cos(k_i l_i) & \frac{\sin(k_i l_i)}{k_i} \\ -k_i \sin(k_i l_i) & \cos(k_i l_i) \end{bmatrix} \begin{bmatrix} f \\ f' \end{bmatrix}_{x=x_i}, \quad (16)$$

where $l_i = x_{i+1} - x_i$ is the thickness of the i -th homogeneous layer and k_i is the wavenumber in it. Situations where Equation (16) appear are mentioned in Table 2 and further discussed in the SM. To propagate a state across the piecewise-defined medium, chain successive matrix multiplications:

$$\begin{bmatrix} f \\ f' \end{bmatrix}_{x=x_N} = \underbrace{\mathbf{T}_N(x_N, x_{N-1}) \dots \mathbf{T}_k(x_k, x_{k-1}) \dots \mathbf{T}_1(x_1, x_0)}_{\mathbf{T}} \begin{bmatrix} f \\ f' \end{bmatrix}_{x=x_0}. \quad (17)$$

\mathbf{T} is called “cumulative” transfer matrix, and it is the product of N “atomic” transfer matrices as in Equation (16), each one associated to a homogeneous piece of the heterogeneous medium.

While the transfer matrix formulation, as in Equation (16), works on amplitudes at each interface, the scattering matrix looks at amplitudes propagating in and out of the stack (recall Figure 1c). To find the relation between the two, one can write: $f = Ae^{-ikx} + Be^{ikx}$, where A, B are the amplitudes of the right-propagating wave and the left-propagating one, respectively, and i is the imaginary unit. In the i -th layer:

$$\begin{bmatrix} A \\ B \end{bmatrix}_{x=x_i} = \begin{bmatrix} e^{ikx_i}/2 & ie^{ikx_i}/2k \\ e^{-ikx_i}/2 & -ie^{-ikx_i}/2k \end{bmatrix} \begin{bmatrix} f \\ f' \end{bmatrix}_{x=x_i} = \mathbf{E}(x_i) \begin{bmatrix} f \\ f' \end{bmatrix}_{x=x_i}, \quad (18)$$

where \mathbf{E} is basis matrix for a second-order linear wave equation (or Helmholtz-type problem) in 1D. hence, the amplitudes of the outgoing waves (at x_N) in terms of the incoming waves (at x_0):

$$\begin{bmatrix} A_R \\ B_R \end{bmatrix}_{x=x_N} = \mathbf{E}(x_N) \mathbf{T}(x_N, x_0) \mathbf{E}(x_0)^{-1} \begin{bmatrix} A_L \\ B_L \end{bmatrix}_{x=x_0} = \mathbf{S}(x_N, x_0) \begin{bmatrix} A_L \\ B_L \end{bmatrix}_{x=x_0}, \quad (19)$$

where \mathbf{S} is the scattering matrix and the subscripts R and L denote wave amplitudes at the right end of the stack and at the left one.

Bloch's theorem and dispersion relations

Floquet/Bloch-type dispersion relations appear widely in one-dimensional photonic [18], phononic [37], acoustic [22], and quantum lattice systems [32, 42]. Bloch's theorem [43] states that for a periodic medium of unit-cell width $L = \sum_i l_i$, the field satisfies

$$\mathbf{T}(\omega) \begin{bmatrix} \text{amplitude} \\ \text{gradient} \end{bmatrix}_{x=L} = e^{ikL} \begin{bmatrix} \text{amplitude} \\ \text{gradient} \end{bmatrix}_{x=L}, \quad (20)$$

so e^{ikL} is an eigenvalue of the transfer matrix $\mathbf{T}(\omega)$. The associated wavenumber k is not known a priori and may be complex. When k is real, waves of that frequency propagate through the periodic structure. When k has positive imaginary part, the wave decays exponentially — this occurs precisely when $|\text{tr } \mathbf{T}(\omega)|/2 > 1$. This condition defines the stop-band, governed by the 1D dispersion relation $\text{tr } \mathbf{T}(\omega) = 2 \cos(kL)$. In such cases, the eigenvalues $\Lambda_{1,2}$ of \mathbf{T} satisfy $\Lambda_1 = 1/\Lambda_2$ and can be written explicitly as

$$\Lambda_{1,2} = \frac{1}{2} \left(\text{tr } \mathbf{T} \pm \sqrt{(\text{tr } \mathbf{T})^2 - 4} \right). \quad (21)$$

A key metric in the stop-band regime is the penetration length (or skin depth), $L_p = L / \ln |\Lambda_1|$, which quantifies the distance over which the wave amplitude decays by a factor of $1/e$ [36].

Operation-count model

Transfer Matrix Method (TMM): For each frequency/wavenumber, the TMM computes a product of N transfer matrices of size 2×2 , giving a total operation count per unit of frequency/wavenumber $\text{Cost}_{\text{TMM}} = \mathcal{O}(N)$.

Path decomposition (full): The number of sign-flip paths through N layers is 2^{N-1} . Each path requires $\mathcal{O}(N)$ operations to compute its amplitude, delay, and phase contribution. Hence, the cost is $\text{Cost}_{\text{Path(full)}} = \mathcal{O}(2^{N-1} \times N)$.

Path decomposition with “pruning” (M-reflection limit): If we restrict the path set to at most M internal reflections, the number of paths becomes $P_M(N) = \sum_{r=0}^M \binom{N-1}{r}$, leading to a cost $\text{Cost}_{\text{Path}(M)} = \mathcal{O}(\cdot N \cdot P_M(N))$. This expression grows polynomially in N for fixed M . For instance $P_2(N) = 1 + (N-1) + \binom{N-1}{2}$.

Supplementary Materials

The code (Jupyter Notebooks) to reproduce the results in Figures 2 to 6 is available at the author’s Github page (github.com/jgarciasuarez/paths). The said repository also contains a a supplementary information file.

References

- [1] Jin, Y. *et al.* The 2024 phononic crystals roadmap. *Journal of Physics D: Applied Physics* **58**, 113001 (2025).
- [2] Lonergan, A. & O’Dwyer, C. Many facets of photonic crystals: From optics and sensors to energy storage and photocatalysis. *Advanced Materials Technologies* **8**, 2201410 (2023).
- [3] Contreras, N., Zhang, X., Hao, H. & Hernández, F. Application of elastic metamaterials/meta-structures in civil engineering: A review. *Composite Structures* **327**, 117663 (2024).

- [4] Zhang, J., Hu, B. & Wang, S. Review and perspective on acoustic metamaterials: From fundamentals to applications. *Applied Physics Letters* **123**, 010502 (2023).
- [5] Mendez, E. E. & von Klitzing, K. *Physics and Applications of Quantum Wells and Superlattices*, vol. 170 (Springer Science & Business Media, 2012).
- [6] Sigalas, M. M. & Economou, E. N. Elastic and acoustic wave band structure. *Journal of Sound and Vibration* **158**, 377–382 (1992).
- [7] Oudich, M., Gerard, N. J., Deng, Y. & Jing, Y. Tailoring structure-borne sound through bandgap engineering in phononic crystals and metamaterials: A comprehensive review. *Advanced Functional Materials* **33**, 2206309 (2023).
- [8] Aki, K. & Richards, P. G. *Quantitative Seismology* (University Science Books, 2002).
- [9] Piña-Flores, J. *et al.* The inversion of spectral ratio H/V in a layered system using the diffuse field assumption (DFA). *Geophysical Journal International* **208**, 577–588 (2016).
- [10] Kuznetsov, S. Seismic waves and seismic barriers. *Acoustical Physics* **57**, 420–426 (2011).
- [11] Faist, J. *et al.* Quantum cascade laser. *Science* **264**, 553–556 (1994).
- [12] Zangeneh-Nejad, F., Sounas, D. L., Alù, A. & Fleury, R. Analogue computing with metamaterials. *Nature Reviews Materials* **6**, 207–225 (2021).
- [13] Hübner, M. *et al.* Optical lattices achieved by excitons in periodic quantum well structures. *Physics Review Letters* **83**, 2841–2844 (1999).
- [14] Maldovan, M. Sound and heat revolutions in phononics. *Nature* **503**, 209–217 (2013).
- [15] Abelès, Florin. Recherches sur la propagation des ondes électromagnétiques sinusoïdales dans les milieux stratifiés - application aux couches minces. *Ann. Phys.* **12**, 596–640 (1950).

- [16] Thomson, W. T. Transmission of elastic waves through a stratified solid medium. *Journal of Applied Physics* **21**, 89–93 (1950).
- [17] Chapman, C. H. Yet another elastic plane-wave, layer-matrix algorithm. *Geophysical Journal International* **154**, 212–223 (2003).
- [18] Li, Z.-Y. & Ho, K.-M. Photonic band structures solved by a plane-wave-based transfer-matrix method. *Physical Review E* **67**, 046607 (2003).
- [19] Mackay, T. G. & Lakhtakia, A. *The Transfer-Matrix Method in Electromagnetics and Optics*. Synthesis Lectures on Electromagnetics (Springer Cham, 2021).
- [20] Jiménez, N., Groby, J.-P. & Romero-García, V. The transfer matrix method in acoustics. In Jiménez, N., Umnova, O. & Groby, J.-P. (eds.) *Acoustic Waves in Periodic Structures, Metamaterials, and Porous Media: From Fundamentals to Industrial Applications*, 103–164 (Springer International Publishing, Cham, 2021).
- [21] Morozov, G. Two forms of transfer matrix for one-dimensional optical structures. *Optical and Quantum Electronics* **55**, 1120 (2023).
- [22] Shen, M. & Cao, W. Acoustic bandgap formation in a periodic structure with multilayer unit cells. *Journal of Physics D: Applied Physics* **33**, 1150 (2000).
- [23] Vinh, P. C., Tuan, T. T. & Capistran, M. A. Explicit formulas for the reflection and transmission coefficients of one-component waves through a stack of an arbitrary number of layers. *Wave Motion* **54**, 134–144 (2015).
- [24] Lipan, O.-Z. & Sabata, A. D. Closed-form analytical solution for the transfer matrix based on pendry-mackinnon discrete maxwell’s equations. *Opt. Express* **33**, 3777–3817 (2025).
- [25] Garcia-Suarez, J. Harmonic decomposition of the trace of 1d transfer matrices in layered media. *Journal of the Mechanics and Physics of Solids* **163**, 104830 (2022).

[26] Garcia-Suarez, J., González-Carbajal, J. & Asimaki, D. Analytical 1d transfer functions for layered soils. *Soil Dynamics and Earthquake Engineering* **163**, 107532 (2022).

[27] González-Carbajal, J., Lemm, M. & Garcia-Suarez, J. On the lowest-frequency bandgap of 1d phononic crystals. *European Journal of Mechanics - A/Solids* **109**, 105466 (2025).

[28] Shi, Y., Li, W., Raman, A. & Fan, S. Optimization of multilayer optical films with a memetic algorithm and mixed integer programming. *Acs Photonics* **5**, 684–691 (2017).

[29] Voti, R. L. Optimization of a perfect absorber multilayer structure by genetic algorithms. *Journal of the European Optical Society-Rapid Publications* **14**, 11 (2018).

[30] Liu, C.-X. & Yu, G.-L. Predicting the dispersion relations of one-dimensional phononic crystals by neural networks. *Scientific Reports* **9**, 15322 (2019).

[31] Yu, G.-L., Song, Z.-G., Cheng, Z.-Y. & Li, Z.-Y. Neural networks for inverse design of phononic crystals. *AIP Advances* **9**, 085223 (2019).

[32] Esaki, L. & Chang, L. L. New transport phenomenon in a semiconductor "superlattice". *Physics Review Letters* **33**, 495–498 (1974).

[33] Kramer, S. L. *Geotechnical Earthquake Engineering* (Prentice Hall Inc., Englewood Cliffs, New Jersey, 1996).

[34] Yeh, P., Yariv, A. & Hong, C.-S. Electromagnetic propagation in periodic stratified media. i. general theory*. *J. Opt. Soc. Am.* **67**, 423–438 (1977).

[35] Griffiths, D. J. & Schroeter, D. F. *Introduction to Quantum Mechanics* (Cambridge University Press, 2018), 3 edn.

[36] Li, K. *Electromagnetic fields in stratified media* (Springer Science & Business Media, 2009).

- [37] Hussein, M. I., Hulbert, G. M. & Scott, R. A. Dispersive elastodynamics of 1d banded materials and structures: Design. *Journal of Sound and Vibration* **307**, 865–893 (2007).
- [38] Steven W, E. *Electromagnetics Vol 2* (Virginia Tech Publishing, 2020).
- [39] Okada, Y. *et al.* Recent progress of seismic observation networks in japan—hi-net, f-net, k-net and kik-net—. *Earth, Planets and Space* **56**, xv–xxviii (2004).
- [40] Feynman, R. P. & Hibbs, A. R. *Quantum Mechanics and Path Integrals* (Dover Publications, Mineola, NY, 2010).
- [41] Jonsson, B. & Eng, S. Solving the schrodinger equation in arbitrary quantum-well potential profiles using the transfer matrix method. *IEEE Journal of Quantum Electronics* **26**, 2025–2035 (1990).
- [42] Kronig, R. D. L., Penney, W. G. & Fowler, R. H. Quantum mechanics of electrons in crystal lattices. *Proceedings of the Royal Society of London. Series A, Containing Papers of a Mathematical and Physical Character* **130**, 499–513 (1931).
- [43] Kittel, C., McEuen, P. & McEuen, P. *Introduction to Solid State Physics*, vol. 8 (Wiley New York, 1996).

Acknowledgments

The support of the Swiss National Science Foundation via Ambizione Grant 216341 is gratefully acknowledged. The author would like to thank Dr. G. Venugopalan for introducing him to the quarter-wavelength method in optics.